ELSEVIER

Available online at www.sciencedirect.com

SCIENCE @ DIRECT®

Applied Surface Science 252 (2006) 3033–3042

applied surface science

www.elsevier.com/locate/apsusc

Nanomechanical characterizations of InGaN thin films

Sheng-Rui Jian [a], Te-Hua Fang [b], Der-San Chuu [a,*]

[a] Institute and Department of Electrophysics, National Chiao Tung University, 1001 Ta Hsueh Road, Hsinchu 300, Taiwan
[b] Institute of Mechanical and Electrochemical Engineering, National Formosa University, Yunlin 632, Taiwan ROC

Received 22 April 2005; received in revised form 4 May 2005; accepted 4 May 2005
Available online 13 June 2005

Abstract

$In_xGa_{1-x}N$ thin films with In concentration ranging from 25 to 34 at.% were deposited on sapphire substrate by metal-organic chemical vapor deposition (MOCVD). Crystalline structure and surface morphology of the deposited films were studied by using X-ray diffraction (XRD) and atomic force microscopy (AFM). Hardness, Young's modulus and creep resistance were measured using a nanoindenter. Among the deposited films, $In_{0.25}Ga_{0.75}N$ film exhibits a larger grain size and a higher surface roughness. Results indicate that hardness decreases slightly with increasing In concentration in the $In_xGa_{1-x}N$ films ranged from 16.6 ± 1.1 to 16.1 ± 0.7 GPa and, Young's modulus for the $In_{0.25}Ga_{0.75}N$, $In_{0.3}Ga_{0.7}N$ and $In_{0.34}Ga_{0.66}N$ films are 375.8 ± 23.1, 322.4 ± 13.5 and 373.9 ± 28.6 GPa, respectively. In addition, the time-dependent nanoindentation creep experiments are presented in this article.
© 2005 Elsevier B.V. All rights reserved.

Keywords: InGaN; XRD; AFM; Nanoindentation; Creep

1. Introduction

The III-nitride wide-band-gap semiconductors are the most promising materials for constructing optoelectronic and electronic devices [1,2]. Among the materials, ternary InGaN alloys which cover the direct-band-gap energy ranging from 1.9 eV (InN) to 3.4 eV (GaN) are crucial and functional materials for GaN-based blue/UV light emitters/lasers and high-power electronic devices [3,4]. Although many works have been focused on the optoelectronic characteristics of InGaN alloys, however, their mechanical properties are almost ignored. InGaN alloys have been used in the form of thin films in optoelectronic and electronic devices. Mechanical properties of materials are size-dependent. Thin films may have different mechanical properties from their bulk materials. A precise measurement of the mechanical properties of InGaN thin films is required to use them as structural/functional elements in devices. Nanoindentation has been widely used for charactering the mechanical properties of solid surfaces and thin films [5,6]. Among the mechanical properties of interest, hardness, Young's modulus, elastic/plastic deformation

* Corresponding author. Tel.: +886 37261111x56105; fax: +886 35725230.
E-mail address: dschuu@mail.nctu.edu.tw (D.-S. Chuu).

0169-4332/$ – see front matter © 2005 Elsevier B.V. All rights reserved.
doi:10.1016/j.apsusc.2005.05.019

behavior and creep resistance can be obtained from nanoindentation testing.

Recently, the indentation-induced plastic behaviors and mechanisms of III–V semiconductors have been discussed [7] in more detail by means of atomic force microscopy (AFM), plane-view and cross-sectional transmission electron microscopy (XTEM); in particular, the effects of alloy strengthening of $In_xGa_{1-x}As$/GaAs were also investigated. To our best knowledge, however, there are no reports on the mechanical properties of InGaN thin films have been made until now.

In this study, InGaN thin films with different indium concentrations were deposited by low-pressure metal-organic chemical vapor deposition (MOCVD). We report, for the first time to our knowledge, the hardness, Young's modulus and creep resistance of InGaN thin films. Nanoindentation deformation behavior of the deposited films was studied by analyzing the nanoindentation load–displacement curves and post-indentation imaging of the indentation impressions. Changes in mechanical properties for the deposited films are discussed in conjunction with deposition temperature, crystalline structure, grain size and surface morphology.

2. Experimental details

The $In_xGa_{1-x}N$ films were grown on sapphire substrate by horizontal low-pressure MOCVD. Prior to material growth, the sapphire substrate was annealed/cleaned to remove surface residual stress and impurities in H_2 gas at 1120 °C for 10 min. Trimethylgallium (TMGa), trimethylindium (TMIn) and ammonia (NH_3) were used as source precursors for gallium, indium and nitrogen, respectively. A 25 nm thick GaN nucleation layer was first deposited at 520 °C for 4 min on the sapphire substrate. The substrate temperature was then raised to 1120 °C to grow a 2 μm thick undoped GaN layer. Finally, a 400 nm thick $In_xGa_{1-x}N$ film was grown on the undoped GaN layer. During growth of the $In_xGa_{1-x}N$ thin films, reactor pressure was kept constant at 200 mbar and input flow rates of ammonia, TMGa and TMIn were kept at 12, 26.5 and 25.5 μmol/min, respectively. To obtain different In concentrations, deposition temperature was varied from 730 to 790 °C. The In concentration in the deposited thin films was obtained by separating GaN and InGaN peaks in X-ray diffraction (XRD) spectra using Vegard's law [8].

Crystalline structure of the deposited InGaN films was characterized using a Bede QC200 X-ray diffractometer with Cu Kα irradiation at 40 kV and 0.4 mA. Surface morphology of the deposited films was investigated by using a Veeco/TM CP-R atomic force microscopy (AFM).

Hardness and the elastic modulus were calculated from the load–displacement (*P*–*h*) data obtained by nanoindentation using a TroboScope nanomechanical testing systems (Hysitron Inc.). The Hysitron nanoindenter monitors and records the load and displacement of the indenter, a diamond Berkovich three-sided pyramid, with a force resolution of about 1 nN and displacement resolution of about 0.1 nm. All nanoindentation tests were performed when the thermal drift dropped down to 0.01 nm/s. The thermal drift effects were corrected for each test using a holding segment in the air before indentation. The indentation impressions were then imaged in situ using the same indenter tip. Five indentations were made on each specimen. A typical indentation experiment consists of four subsequent steps: approaching the surface; loading to peak load at a loading rate of 10 μN/s; holding the indenter at peak load for 5 s; finally unloading completely. The hold step was included to avoid the influence of creep on the unloading characteristics since the unloading curve was used to obtain the elastic modulus of a material. For more details on nanoindentation experimental techniques, please see references [5,6].

The indentation *P*–*h* data obtained at each depth were analyzed to determine the hardness, *H*, and elastic modulus, *E*, by using the Oliver and Pharr method [9]. In this method, the hardness and modulus are determined as following.

Nanoindentation hardness is defined as the indentation load divided by the projected contact area of the indentation. It is the mean pressure that a material will support under load. From the *P*–*h* curve, hardness can be obtained at the peak load as:

$$H = \frac{P_{max}}{A} \tag{1}$$

where *A* is the projected contact area.

The elastic modulus was calculated using the Oliver–Pharr data analysis procedure [9] beginning by

fitting the unloading curve to a power-law relation defined as:

$$\frac{1}{E_r} = \left(\frac{1-v^2}{E}\right)_{\text{specimen}} + \left(\frac{1-v^2}{E}\right)_{\text{indenter}} \quad (2)$$

which is calculated from the contact stiffness S using the following formula:

$$S = \frac{2\beta}{\sqrt{\pi}} E_r \sqrt{A} \quad (3)$$

The above equation is derived from Sneddon's solution [10] to the elastic contact problem between a half space and axi-symmetric punch; and E and v in Eq. (3) are the elastic modulus and Poisson's ratio for the specimen and, β is a constant which depends on the geometry of the indenter ($\beta = 1.034$ for a Berkovich indenter) [9]. The contact area A is calculated from the contact depth h_c through a pre-calibrated shape function $A = f(h_c)$ of the indenter, and h_c is given by:

$$h_c = h_{max} - \varepsilon \frac{P_{max}}{S} \quad (4)$$

where h_{max} is the maximum indenter penetration depth, and ε is a constant depending on the indenter geometry ($\varepsilon = 0.72$ for the Berkovich indenter tip). For diamond, $E_i = 1141$ GPa and $\nu_i = 0.07$ [9].

In a nanoindentation creep test, a constant load of 1 mN is applied to the indenter and the change in indentation depth (size) is monitored as a function of time. The depth-sensing nanoindenter used in this study can in situ measure indentation depth as a function of holding time.

3. Results and discussion

3.1. Structural and surface characterization

Fig. 1 shows the XRD spectra and AFM images of the InGaN films deposited at 790, 760 and 730 °C, respectively. The InGaN and GaN peaks are observed in the XRD spectra and these two peaks do not shift while the In concentration is increased. The In concentrations in the InGaN films deposited at 790, 760 and 730 °C are 25, 30 and 34%, respectively. The concentrations were obtained by separating the GaN and InGaN peaks in XRD spectra using Vegard's law [8]. Broadness of the InGaN peak is attributed to alloying and finite domain size effects [11]. From Scherrer's formula [12], the grain sizes for the $In_{0.25}Ga_{0.75}N$, $In_{0.3}Ga_{0.7}N$ and $In_{0.34}Ga_{0.66}N$ films were calculated to be 9.9, 9.8 and 8.6 nm, respectively, indicating a decrease in grain size with decreasing deposition temperature.

The AFM images of the deposited InGaN films show island-like surface morphology. The surface roughness (RMS) values of the $In_{0.25}Ga_{0.75}N$, $In_{0.3}Ga_{0.7}N$ and $In_{0.34}Ga_{0.66}N$ thin films are 5.3, 2.9 and 2.6 nm, respectively, showing a trend of decrease in surface roughness with decreasing deposition temperature. With decreasing deposition temperature, mobility of the surface atoms decreases, resulting in smaller grain size and smoother surface.

3.2. Hardness and Young's modulus

A representative P–h curve of the $In_{0.25}Ga_{0.75}N$ film obtained at an indentation load of 1.5 mN and an AFM indent image of the indent are shown in Fig. 2. Sink-in is found around the indentation mark. As reported by Bolshakov and Pharr [13], all materials with a ratio of h_f/h_{max} below 0.7 exhibit sink-in; while the materials with a ratio of h_f/h_{max} above 0.7 show pile-up [14]. The shape of the indentation revealed that the sides of the indentation recover more than the corners. This is probably due to the difference in stress concentration induced in the material during the nanoindentation process. The stress concentration is greater at the corners of a Berkovich tip than its sides.

The effects of pile-up/sink-in on the hardness and Young's modulus can be neglected due to the fact that Young's modulus remains essentially constant over the indentation penetration depth. Fig. 3 shows that the hardness and Young's modulus as a function of indenter penetration depth. Young's moduli for the $In_{0.25}Ga_{0.75}N$, $In_{0.3}Ga_{0.7}N$ and $In_{0.34}Ga_{0.66}N$ films are 375.8 ± 23.1, 322.4 ± 13.5 and 373.9 ± 28.6 GPa, respectively. Young modulus of the GaN layer is 314.9 ± 40.6 GPa [15].

Hardness is one of material's characteristic properties that can be used to assess the film's plastic behavior. The hardness for the $In_{0.25}Ga_{0.75}N$, $In_{0.3}Ga_{0.7}N$ and $In_{0.34}Ga_{0.66}N$ films are 16.6 ± 1.1, 16.5 ± 1.0 and 16.1 ± 0.7 GPa, respectively. Compared with the previous study [15], the hardness of $In_xGa_{1-x}N$ is

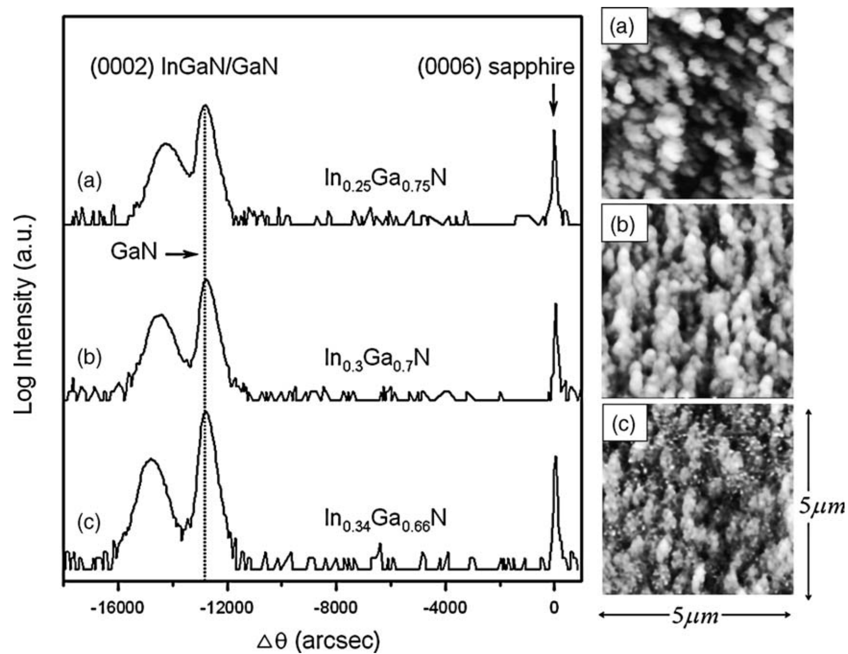

Fig. 1. XRD spectra (left) and AFM images (right) of InGaN films deposited at growth temperatures of 790, 760 and 730 °C for In-content of (a) 25%; (b) 30%; and (c) 34%, respectively.

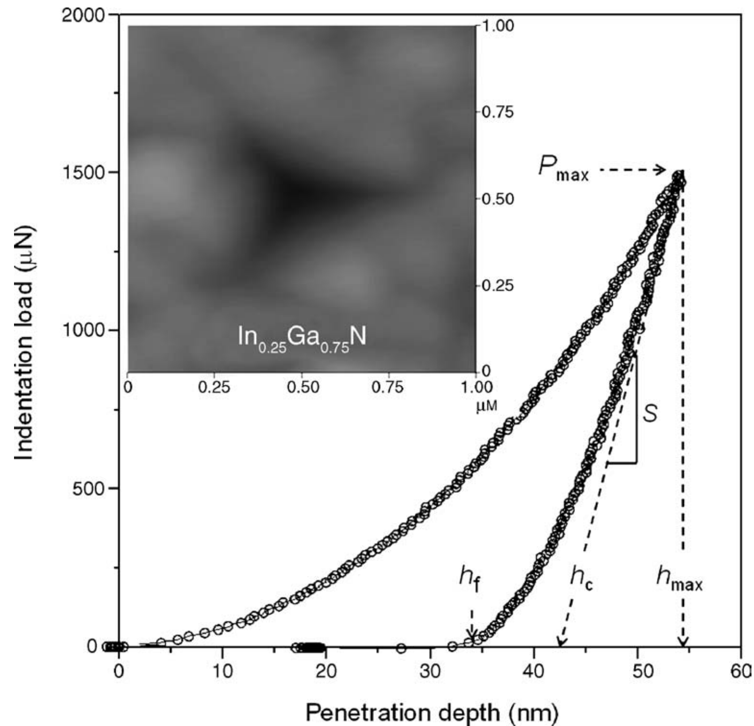

Fig. 2. AFM micrograph of a Berkovich indentation on $In_{0.25}Ga_{0.75}N$ film obtained at the indentation load of 1500 μN and *P–h* curve on the surface and in an indentation.

lower than that of the GaN (19.3 ± 2.1 GPa). This indicates that the higher the indium content is the lower the hardness will be. In addition, the hardness slightly decreases with an increase in indentation depth or indentation load. This may be due to an indentation size effect (ISE) whereby the measured hardness increases as indentation load is decreased [15–17]. ISE has been attributed to varieties of contributions, such as dislocation nucleation [19], specimens surface energy [20], statistical measurements errors [21] and surface and plastic strain energy dissipation [18].

In Fig. 3, it can be seen that the hardness values decreased slightly (from 16.8 ± 0.8 to 16.2 ± 0.8 GPa) as the indium content is increased at a penetration depth of ~52 nm. The variation of the indium content is very small; to obtain more precise information, it is essential to measure specimens with various indium contents to conclude the tendency. Another explanation is that the variation of hardness may be caused by surface roughness/asperities. The penetration depth is often of the same order of magnitude as the grain size of the specimen (it was noticed that the plastic zone size is ~350 nm that is about 35 grains at h_c = 50 nm) and the location of grain boundaries relative to the indenter can strongly influence the measurement of the mechanical characterizations, which leads to an inaccurate measurement of hardness of specimen. Bobji et al. [22] found that the roughness manifestly increases the scatter of hardness, especially at small penetration depths by finite element analysis. The material was measured to be significantly harder at smaller penetration depth. Zhang and Xu [23] investigated the effects of surface stress on the nanoindentation mechanical property measurements. They pointed out that the contribution of surface work to nanoindentation is associated with the apparent surface stress and the geometry of the indenter tip. The depth-dependent hardness can be given by:

$$H - \sigma_0 = \alpha \frac{f}{h_c} \quad (5)$$

where σ_0 is denoted as the internal stress of films and the right hand side of Eq. (5) has drawn an analogy with the previously study [23]. The numerical factor α is 1.1827 and f represents the apparent surface stress.

Fig. 4 illustrates the hardness as a function of the reciprocal penetration depth for the InGaN thin films. The variation in the depth-dependent hardness with various indium contents may be caused by the anisotropic behavior of the apparent surface stress. The results indicate that the main factor f for the $In_{0.25}Ga_{0.75}N$, $In_{0.3}Ga_{0.7}N$ and $In_{0.34}Ga_{0.66}N$ films is 263.4, 213.7 and 183.8 J/m^2, respectively. The rougher the surface, the higher the surface stress value of f is. The rougher surface may consume more energy during nanoindentation and thus leads to a higher apparent surface stress.

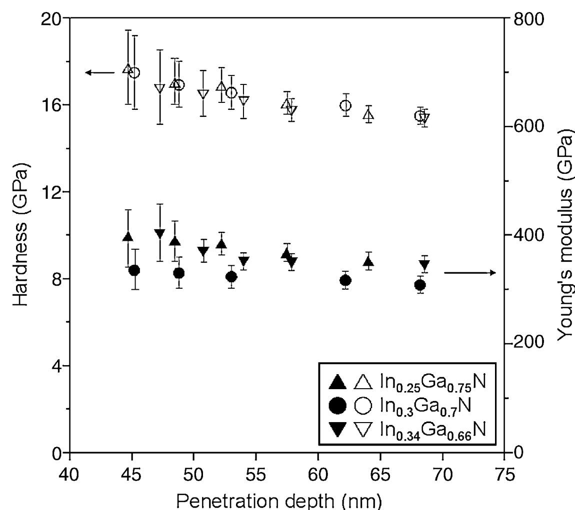

Fig. 3. Hardness and Young's modulus of InGaN thin films as a function of penetration depth.

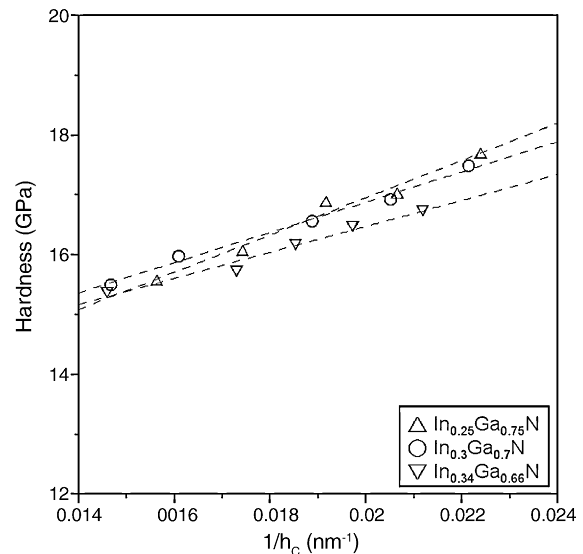

Fig. 4. Hardness vs. the reciprocal penetration depth for InGaN thin films.

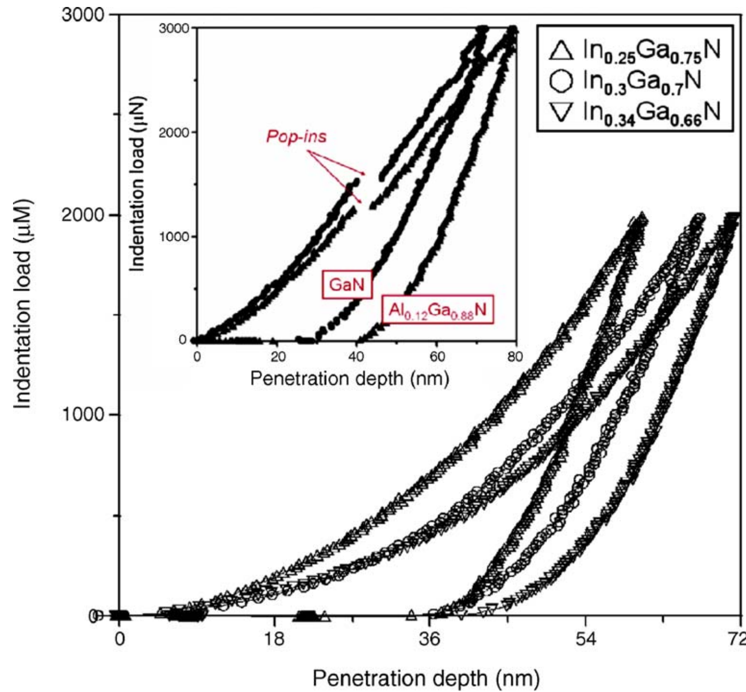

Fig. 5. *P–h* curves measured during indentation of InGaN thin films. The schematic *P–h* curve to illustrate the pop-in events of GaN and $Al_{0.12}Ga_{0.88}N$ thin films in the insert [15].

A discontinuity in the loading curve, so called ''pop-in'' event was observed in several studies of III-nitride semiconductor materials [15,24]. This phenomenon was attributed to very poor defect density prior to nanoindentation tests so that the onset of plasticity requires load sufficient for dislocation nucleation and propagation. In contrast, epitaxial layers are expected to contain more defects like surface steps [25] that are known to facilitate the onset of plasticity [26]. In fact, during this research, no pop-in event was discovered in Fig. 5.

The maximum shear stress τ_m can be expressed through the mean contact pressure (p_a) as following from Hertz contact theory [27]:

$$\tau_m = 0.465\,p_a = 0.47\frac{16}{9}\frac{E_{eff}^2 \times h_c^2}{\pi \times P_{max}} = 0.465\frac{4E_{eff}}{3\pi}\sqrt{\frac{h_c}{R}} \tag{6}$$

where an indentation load (P_{max}) and the penetration depth (h_c) at known tip radius of the indenter or effective elastic modulus of films (E_{eff}). The τ_m of the InGaN thin films ranges from 48.3 to 57.1 GPa. The theoretical shear strength τ_T of indented materials may be approximated as [28]:

$$\tau_T = \frac{\mu_S}{2\pi} = \frac{E_f}{4\pi(1+\upsilon_f)} \tag{7}$$

where μ_S is the shear modulus. The theoretical shear strength τ_T for the InGaN thin films ranges from 19.8 to 23.2 GPa. The difference between τ_m and τ_T is due to the experimental scatter, residual stresses in films, defects or grain boundaries and surface roughness.

3.3. Creep resistance

The time-dependent plasticity behavior is often observed in nanoindentation tests due to continuous deformation occurring during holding. The holding time at the maximum load was used to show the creep effects of $In_{0.34}Ga_{0.66}N$ film seen in Fig. 6(a). At a constant loading rate, the indentation load increased until arriving at a maximum load, subsequently there is an increase of the penetration depth from h_i to h_e, i.e.

the creep length during the nanoindentation process at a hold time.

Fig. 6(b) depicts the *P–h* curves of the $In_{0.3}Ga_{0.7}N$ film at an indentation load of 1000 μN and at a 10 μN/s loading rate. The hold times are 0.1, 15 and 30 s. It can be seen that increasing the holding time at the maximum indentation load increases the penetration depth. The longer holding time is found to produce a deeper penetration depth into the specimen. This is due to the nanoindentation creep phenomena.

The extent of the increased creep length decays with increasing the holding time, therefore, the hardness shows a decreasing tendency for the InGaN thin films. The longer holding time yields more creep-

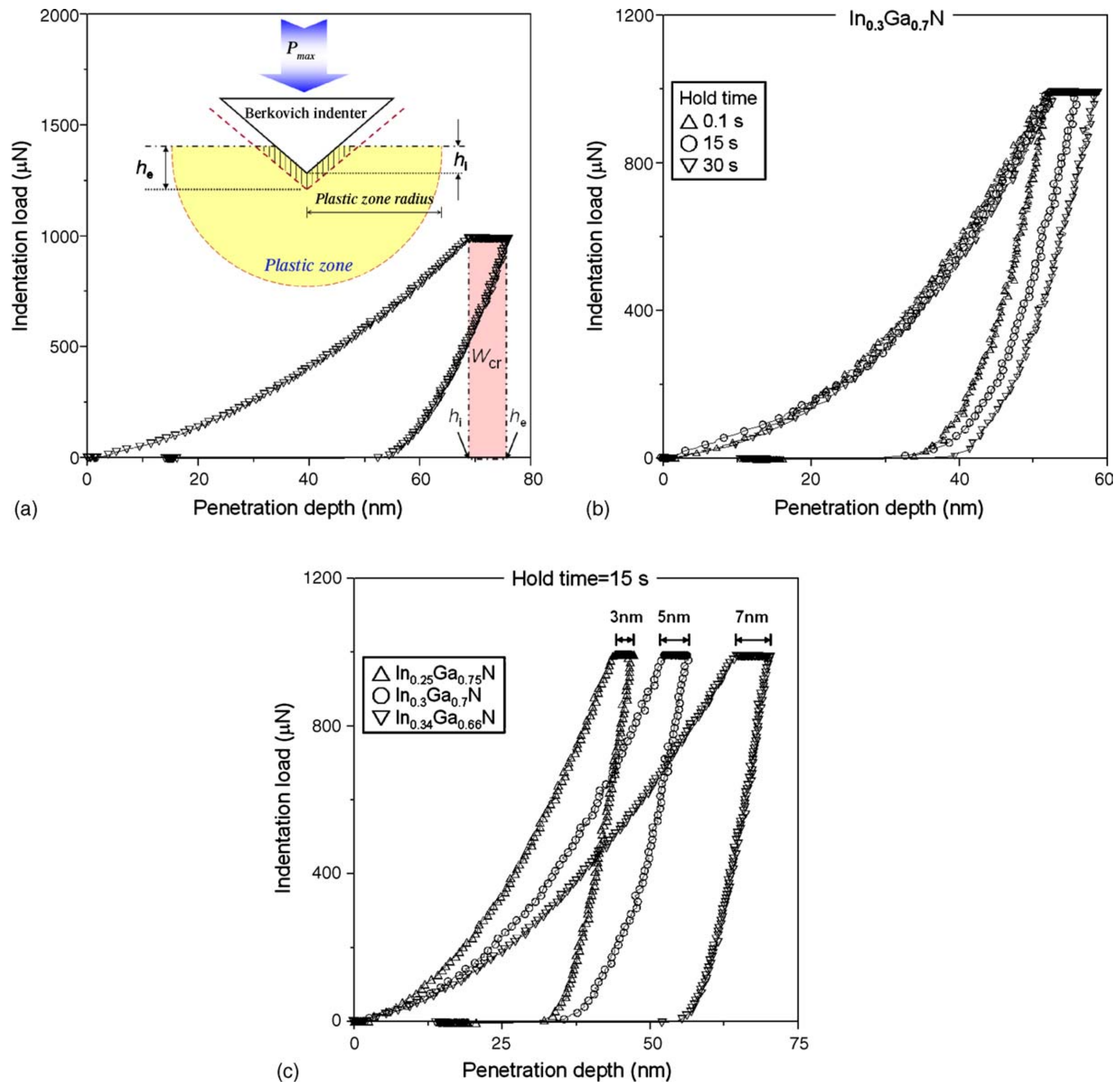

Fig. 6. (a) Schematic diagram of indentation creep *P–h* curve for $In_{0.34}Ga_{0.66}N$ film obtained at an indentation load of 1000 μN and at the holding time of 30 s. The work of indentation creep (W_{cr}) done is represented by the creep hold time area (between h_i and h_e at an indentation load of 1000 μN). (b) *P–h* curves for various hold time on $In_{0.3}Ga_{0.7}N$ film. (c) *P–h* curves for InGaN thin films at the same hold time of 15 s. All cases are measured at an indentation load of 1000 μN and a loading rate of 10 μN/s.

deformed region; thus, the higher plastic deformation work (W_{cr}) would be generated. The phenomenon of creep-induced deformation is caused by dislocation creep behaviors. As shown in Fig. 6(c), the longer creep length displays at the higher indium content; therefore, the $In_{0.34}Ga_{0.66}N$ film exhibits the softer material property and the larger W_{cr} during the nanoindentation observations. Furthermore, the strain sensitivity of the InGaN thin films subjected to nanoindentation creep evaluation will be discussed below.

On the other hand, in the indentation creep experiments, the material underneath the indenter is very often likened to an expanding cavity at which no deformation occurs and an expanding elastic–plastic regime exists (see the insert in Fig. 6(a)). In this small-scale range, the plastic zone was described well by Johnson's cavity model [29] with the plastic zone radius r_P defined as follows:

$$r_p = \left(\frac{3P_{max}}{2\pi\sigma_Y}\right)^{1/2} \tag{8}$$

where σ_Y is the uniaxial yield strength, to describe the complex mechanical problems of fully plastic deformation with a single quantity of $\sigma_Y = H/3$[30] and the factor 3 results essential from geometric considerations [31]. During the holding time of 0.1–30 s, the r_P of $In_{0.25}Ga_{0.75}N$, $In_{0.3}Ga_{0.7}N$ and $In_{0.34}Ga_{0.66}N$ films ranges from 283.6 ± 3.56 to 410.4 ± 2.4 nm, 300.8 ± 2.5 to 415.8 ± 1.1 nm and 302.8 ± 1.6 to 416.4 ± 0.8 nm, respectively. The variation of r_P remains relatively unchanged at the longer holding time. It implies that the plastic work was sustained accumulated in the materials, resulting in the increase in dislocations/microcracks nucleation during the nanoindentation creep processes.

Fig. 7 shows the relationships between the hold time and the hardness and Young's modulus at an applied indentation load of 1000 μN and a loading rate of 10 μN/s. The hardness and Young's modulus slightly decreases at the early stage of holding. As the holding time evolves, the hardness and Young's modulus is decreased. It is believed that the increase in indentation penetration depth is due to the creep effect, thereby resulting in a lower hardness. In this present study, the hardness of $In_{0.25}Ga_{0.75}N$, $In_{0.3}Ga_{0.7}N$ and $In_{0.34}Ga_{0.66}N$ films changes 52.3, 47.6 and 47.1%, respectively. Young's modulus for the $In_{0.25}Ga_{0.75}N$, $In_{0.3}Ga_{0.7}N$ and $In_{0.34}Ga_{0.66}N$ films changes 16.2, 16.5 and 31.2%, respectively. After 25 s holding time, both the hardness and Young's modulus are kept constant.

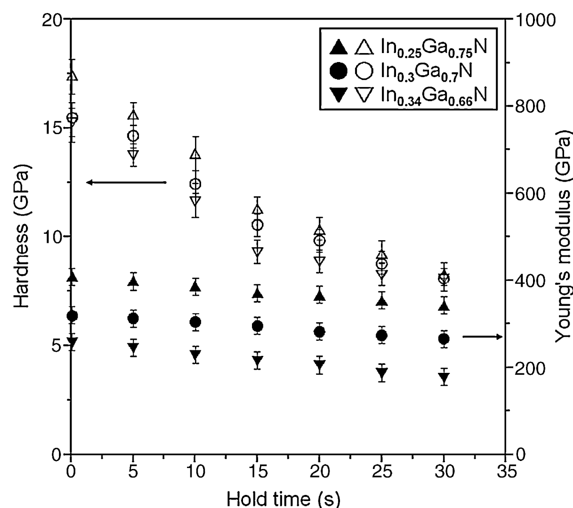

Fig. 7. Hardness and Young's modulus records for InGaN thin films as a function of the holding time (at an indentation load of 1000 μN and a loading rate of 10 μN/s).

In the creep processes, the strain rate $\dot{\varepsilon}_{cr}$ is generally correlated with the normal displacement rate of the indenter divided by the displacement $\dot{h}/h$, i.e.

$$\dot{\varepsilon}_{cr} = k_1\left(\frac{\dot{h}}{h}\right) \tag{9}$$

where k_1 is a material constant and it usually equals to 1. In addition, the constitutive relation of time-dependent creep deformation behavior can be expressed as the power-law [32]:

$$\sigma_{cr} = k_2\dot{\varepsilon}_{cr}^{m_{cr}} \tag{10}$$

where σ_{cr}, m_{cr} and k_2 are denoted as the time-dependent stress, strain rate sensitivity and material constant, respectively. Using Eqs. (9) and (10) the strain rate sensitivity m_{cr} can be calculated as:

$$m_{cr} = \frac{\partial \ln \sigma_{cr}}{\partial \ln \dot{\varepsilon}_{cr}} \tag{11}$$

Fig. 8 shows the plots of the time-dependent indentation stress versus the strain rate data from the InGaN thin films nanoindentation creep experiments. It is a clear indication that the value of $\ln\dot{\varepsilon} \gtrsim -4.4$

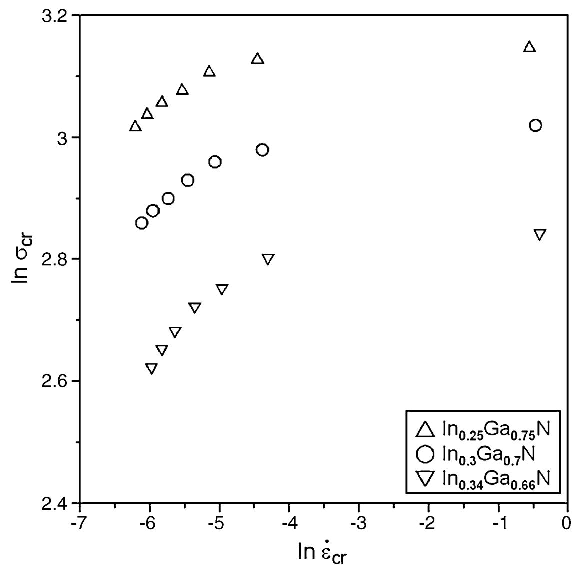

Fig. 8. Logarithmic plots of indentation stress *vs.* strain rate of InGaN thin films.

implies InGaN thin films is largely flat for most part of the plastic deformation and decreased sharply for smaller $\ln\dot{\varepsilon}_{cr}$ during plastic deformation.

In addition, nanoindentation creep tests indicate that the time-dependent behavior is characterized by the strain rate sensitivity. The m_{cr} was calculated by the linear portion of the curves (which was taken from the x-axis at the range of -4 to-6 in Fig. 8) and was displayed in Fig. 9 The m_{cr} increases as the InGaN

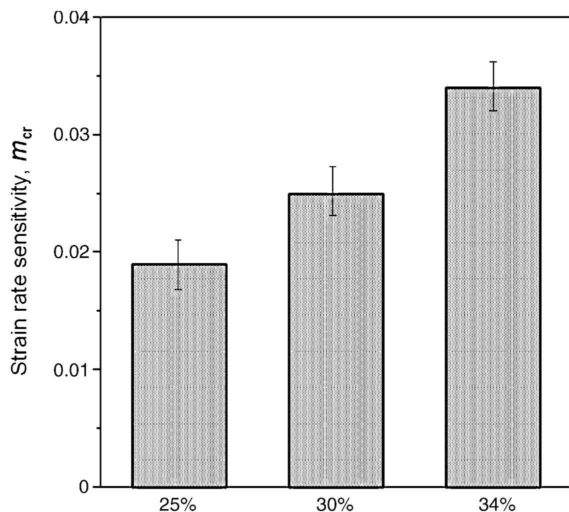

Fig. 9. Strain rate sensitivity m_{eff} at various indium contents.

films with higher indium content. There are two cases of $m_{cr} = 1$ and $m_{cr} \neq 1$ corresponding to plastic deformation behaviors of Newtonian flow and non-Newtonian flow, respectively. In this present work, creep behaviors of the InGaN thin films are denoted by $m \neq 1$, suggesting a non-Newtonian viscous behavior.

4. Conclusions

The structural features and nanomechanical properties of the InGaN thin films with different In-content produced by MOCVD were investigated using the XRD, AFM and nanoindentation techniques. The following results were obtained:

(1) XRD analysis and AFM micrographs show no evidence of phase separation for InGaN thin films; also with a relatively smooth surface.
(2) Nanoindentation results indicate that Young's modulus has no varied significantly and, at lower indentation depths, a slightly increasing hardness is found, as for the ISE on the InGaN thin films. Good agreement is found in the experimental results of depth-dependent hardness, indicating that the surface effects play an important role in depth-dependent hardness.
(3) In nanoindentation creep measurements, both the hardness and Young's modulus of the InGaN thin films decrease as the holding time is increased, resulting in 47.1–52.3% reduction in the hardness and 16.2–31.2% reduction in Young's modulus. The contact area increases as a Berkovich indenter penetrates InGaN thin films while the indentation load is held constant, the hardness decreases as the tests proceeds, with a corresponding decrease in the indentation creep strain rate.
(4) The creep strain behaviors can be found obviously at a "critical point" of $\ln\dot{\varepsilon}_{cr} \approx -4.4$. Also, the strain rate sensitivity m_{cr} increases with increasing the indium content and the non-Newtonian viscous behavior was observed.

Acknowledgement

Authors would like to thank Prof. X. Li, Department of Mechanical Engineering, University of South

Carolina, USA, for his helpful discussions, and this work was partially supported by the National Science Council of Taiwan, under Grant Nos. NSC93-2218-E218-005 and NSC94-M2120-009-002.

References

[1] M.A. Khan, A. Bhattarai, J.N. Kuznia, D.T. Olson, Appl. Phys. Lett. 63 (1993) 1214.
[2] S. Nakamura, M. Senoh, S. Nagahama, N. Iwasa, T. Yamada, T. Matsushita, Y. Sugimoto, H. Kiyoku, Appl. Phys. Lett. 69 (1996) 4056.
[3] S. Nakamura, G. Fasol, The Blue Laser Diode, Springer, Berlin, 1997.
[4] B. Gil (Ed.), Ground III Nitride Semiconductor Compounds: Physics and Applications, Oxford University Press, Oxford, New York, 1998.
[5] B. Bhushan, X. Li, Int. Mater. Rev. 48 (2003) 164.
[6] X. Li, B. Bhushan, Mater. Charact. 48 (2002) 36.
[7] E.L. Bourhis, G. Patriarche, Prog. Cryst. Growth Charact. Mater. 47 (2003) 1.
[8] Z. Qin, Z. Chen, Y. Tong, S. Lu, G. Zhang, Appl. Phys. A 74 (2002) 655.
[9] W.C. Oliver, G.M. Pharr, J. Mater. Res. 7 (1992) 1564.
[10] I.N. Sneddon, Int. J. Eng. Sci. 3 (1965) 47.
[11] R.W. Vook, in: J.W. Matthews (Ed.), Epitaxial Growth, Academic Press, New York, 1975.
[12] B.D. Cullity, Elements of X-ray Diffraction, Addison-Wesley, Reading, MA, 1978.
[13] A. Bolshakov, G.M. Pharr, J. Mater. Res. 13 (1998) 1049.
[14] R. Smith, D. Christopher, S.D. Kenny, A. Richter, B. Wolf, Phys. Rev. B 67 (2003) 245405.
[15] S.R. Jian, T.H. Fang, D.S. Chuu, J. Electron. Mater. 32 (2003) 496.
[16] W.D. Nix, H. Gao, J. Mech. Phys. Solids 46 (1998) 411.
[17] A.A. Elmustafa, D.S. Stone, Acta Mater. 50 (2002) 3641.
[18] W.W. Gerberich, N.I. Tymiak, J.C. Grunlan, M.F. Horstemeyer, M.I. Baskes, J. Appl. Mech. 69 (2002) 433.
[19] N. Gane, J.M. Cox, Philos. Mag. 22 (1970) 881.
[20] H. Hirao, M. Tomozawa, J. Am. Ceram. Soc. 70 (1987) 497.
[21] F.G. Yost, Metall. Trans. A 14 (1983) 947.
[22] M.S. Bobji, S.K. Biswas, J.B. Pethica, Appl. Phys. Lett. 71 (1997) 1059.
[23] T.Y. Zhang, W.H. Xu, J. Mater. Res. 17 (2002) 1715.
[24] J.E. Bradby, S.O. Kucheyev, J.S. Williams, J.W. Leung, M.V. Swain, P. Munroe, G. Li, M.R. Phillips, Appl. Phys. Lett. 80 (2002) 383.
[25] G. Patriarche, F. Glas, G.L. Roux, L. Largeau, A. Mereuta, J.L. Benchimol, J. Cryst. Growth 221 (2000) 12.
[26] S. Brochard, J. Rabier, J. Grilhe, Eur. Phys. J. AP 2 (1998) 99.
[27] D. Lorenz, A. Zeckzer, U. Hilpert, P. Grau, H. Johansen, H.S. Leipner, Phys. Rev. B 67 (2003) 172101.
[28] T.H. Courtney, Mechanical Behavior of Materials, McGraw Hill, New York, 2000.
[29] W. Zielinski, H. Huang, W.W. Gerberich, J. Mater. Res. 8 (1993) 1300.
[30] D. Tabor, The Hardness of Metals, Oxford University Press, Oxford, UK, 1951.
[31] K.L. Johnson, Contact Mechanics, Cambridge University Press, Cambridge, UK, 1985.
[32] A. Juhasz, P. Tasnadai, I. Kovacs, J. Mater. Sci. Lett. 5 (1996) 35.